Research Paper

EARTHQUAKE SPECTRA

Earthquake Spectra
1–26

DOI: 10.1177/87552930251378782
journals.sagepub.com/home/eqs
Sage

Seismic fragility assessment of confined masonry houses in Colombia

Jorge Archbold, M.EERI[1,2], Julian Carrillo, M.EERI[2,3], Johnatan Orjuela Mejia[4], and Jefferson Piedrahita[5]

Abstract

Confined masonry (CM) houses are widely used in low- and mid-rise houses worldwide, especially in countries with emerging economies. CM emerged in Latin America as a response to the severe damage observed in unreinforced masonry buildings following significant earthquakes in the early twentieth century. In Colombia, CM construction dates back to the 1930s, with houses up to five stories tall. A key challenge in seismic risk estimation is predicting the behavior of prevalent construction typologies in a region to inform risk mitigation and management strategies. As a part of a larger project called the National Seismic Risk Model for Colombia, this study presents a seismic fragility assessment of CM houses, evaluating the effects of masonry strength, masonry unit type, wall density, construction quality, and number of stories. A total of 72 archetype houses, representative of Colombian CM structures, were analyzed across low, intermediate, and high seismicity zones. Nonlinear models were proposed and calibrated using quasi-static cyclic tests on confined masonry walls and shaking table tests on scaled buildings. For each archetype, nonlinear time history analyses were conducted in OpenSees, using approximately 370 hazard-consistent ground-motion records to represent the hazard at each site of interest. The results from these structural analyses are then combined with damage information to obtain fragility curves for this building typology. The fragility results of this study, combined with vulnerability functions, will serve as inputs to calculate risk metrics later on as part of the National Seismic Risk Model for Colombia. The present work provides a region-specific fragility assessment, calibrated with local experimental data, which enhances its applicability within Colombia and potentially to other Latin American

[1]Department of Civil and Environmental Engineering, Universidad Del Norte, Barranquilla, Colombia
[2]Colombian Earthquake Engineering Research Network, CEER, Medellín, Colombia
[3]Universidad Militar Nueva Granada, Bogota, Colombia
[4]École Polytechnique Fédérale de Lausanne, Lausanne, Switzerland
[5]Universidad Tecnológica de Bolivar, Cartagena, Colombia

Corresponding author:
Jorge Archbold, Department of Civil and Environmental Engineering, Universidad del Norte, Km. 5 vía Puerto Colombia, Barranquilla, Atlantico 081007, Colombia.
Email: jarchbold@uninorte.edu.co

countries with similar construction practices and standards. These findings can contribute directly to national seismic risk mitigation initiatives.

Keywords
Seismic fragility, confined masonry, fragility functions, nonlinear time history analysis, probabilistic seismic assessment

Date received: 20 January 2025; accepted: 5 August 2025

Introduction

Toward the end of the last century, the structural engineering community learned that even moderate-magnitude earthquakes could lead to substantial societal impacts (Chung, 1996; Eguchi et al., 1998). For example, in Colombia, the magnitude 6.1 *Coffee Region* earthquake in 1999 resulted in significant damage due to its proximity to densely populated areas like Armenia and Pereira, its shallow depth, and the vulnerability of the building stock at that time. The National Administrative Department of Statistics reported approximately 1200 fatalities, 8500 injuries, and the displacement of more than 159,000 people, while 36,000 dwellings collapsed and 43,500 dwellings sustained minor to moderate damage (DANE, 1999). Despite updates to seismic design standards, the level of structural damage and associated economic losses (Asfura and Flores, 1999), estimated at approximately US$1.9 billion (Restrepo and Cowan, 2000) were unacceptably high.

In response to the need for better national-scale risk information, the Colombian Geological Survey conceived and funded the Seismic Risk Model for Colombia (MNRS, for its initialism in Spanish) in 2021. The initiative aims to assess the impacts and potential consequences of future earthquakes, thereby supporting emergency response, recovery, and reconstruction policies. One of the objectives of the MNRS is to estimate the fragility and vulnerability functions of commonly used structural typologies, such as reinforced concrete (RC) frame buildings, RC wall buildings, reinforced masonry (RM), unreinforced masonry (URM), partially confined masonry, and CM. This study focuses on one such typology: CM houses. Specifically, it examines engineered buildings designed according to seismic code provisions, and the results are not applicable to informal or non-engineered housing. Although formal seismic codes have existed in Colombia for roughly four decades, enforcement largely depends on socioeconomic conditions, with non-engineered construction still common in lower-income communities (Acevedo et al., 2020).

CM is a construction typology widely used in low- and mid-rise buildings throughout Latin America, Europe, and Asia. According to Yepes-Estrada et al. (2017) masonry structures represent over 55% of the building stock in Latin America, where 31% correspond to URM, 22% to CM and 2% to RM buildings. CM structures comprise masonry walls enclosed by RC confining elements (Figure 1). Typically, the masonry wall is constructed first, followed by the casting of the RC members. This construction method distinguishes CM from both URM, which lacks confinement, and RM, which typically integrates reinforcement within the wall itself. CM walls emerged as an alternative construction system in different countries to improve the poor behavior observed in URM houses (Meli et al., 2011). For example, CM houses were built in Mexico and Chile following the 1940 Mexico City and 1928 Talca earthquakes. In Colombia, the first records of one- to five-story CM houses date back to the 1930 (Yamín and García, 1992).

Figure 1. Example of CM houses in Colombia.
Images adapted from Google Street View (Google LLC, 2023).

To support national risk assessments like the MNRS, various methodologies have been developed to derive seismic fragility functions. Martins and Silva (2021) summarize these methods, which span from detailed nonlinear modeling approaches such as the 3D finite element models of RC frame buildings subjected to nonlinear dynamic analyses (Martins et al., 2016; Ulrich et al., 2014), to more simplified and computationally efficient procedures using single-degree-of-freedom or multi-degree-of-freedom oscillators subjected to nonlinear static analyses (Silva et al., 2013; Vamvatsikos and Allin Cornell, 2006). While national-scale risk models often rely on simplified numerical models (Dolšek, 2011; Martins and Silva, 2021; Villar-Vega et al., 2017), this study adopts a different approach using 3D nonlinear time history (NLTH) analyses of CM building models to derive fragility functions for building classes.

Several authors have reviewed the different strategies developed to model the nonlinear seismic response of CM structures (Borah et al., 2021; Marques et al., 2020; Rankawat et al., 2021). These approaches range from detailed micro-models to simplified macro-models. Micro-models capture the interaction between units and mortar with high accuracy but are rarely used due to their high computational cost. Simplified macro-models such as wide column, strut-and-tie, or equivalent strut approaches are more efficient but often fail to represent key aspects like axial load effects or composite wall action. To address these limitations, Borah et al. (2021) proposed an equivalent strut model that includes a vertical element to simulate gravity load transfer and a diagonal element to represent lateral resistance. This model is adopted in this study as a balance between physical realism and computational efficiency.

Fragility curves for CM buildings have been developed by several authors from numerical and experimental analysis (GEM, 2022; Gonzales et al., 2020; Lovon et al., 2018; Martins and Silva, 2021; Rota et al., 2010). The values of these fragility curves are highly influenced by the mechanical properties of the masonry, the wall's density of the buildings and the axial load considered in the analysis. Unlike previous research, which often assumes simplified or idealized configurations, this work incorporates irregular geometries and realistic material laws to better capture the physical mechanisms governing seismic response.

As previously mentioned, this article develops seismic fragility curves for CM houses representative of the Colombian building stock. For this purpose, first, representative archetypes were first developed using an analysis of typical CM houses across the country, reflecting regional variations in construction practices and materials. These archetypes were then designed following the requirements of Chapter D of the latest Colombian seismic design code, NSR-10 (AIS, 2010), to ensure compliance with current structural standards. A total of 72 archetypes were defined and modeled using OpenSees (McKenna et al., 2010), with a modified version of the equivalent Vertical-Diagonal (V-D) strut model proposed by Borah et al. (2021). The numerical model was validated using experiments from the literature and validated at the element and structure levels. The response of these archetype buildings was evaluated through NLTH analyses, utilizing a hazard-consistent ground motion set selected based on the Conditional Scenario Spectra (Arteta and Abrahamson, 2019). This approach allowed for the development of fragility curves specific to Colombian CM buildings, which represent a valuable input to the MNRS project.

Database compilation

The assessment of CM behavior using fragility curves at a regional level requires selecting representative housing prototypes, hereinafter referred to as archetype houses. Fragility curves can then be developed using numerical results obtained from a numerical analysis of the response of the archetype houses at various seismic demand levels. A comprehensive database of 34 CM houses, ranging from one to four stories, was compiled. The sources used to create the database included drawings and structural design documents for CM houses provided by local structural engineers and a literature review of master's and doctoral theses as well as peer-reviewed journal articles (Acevedo et al., 2020; Arias Acosta, 2005; Borah, 2021; Maldonado Rondón and Chio Cho, 2008; Yamín and García, 1992) aimed at assessing the behavior of CM houses under lateral loads. After the assembly of the database, a statistical analysis was performed to characterize representative values of relevant system properties, such as floor area, wall thickness, wall densities in each direction, number of stories, and inter-story height, among others. This analysis identified trends and average values for several construction attributes that were later used to define archetype houses.

Furthermore, a statistical analysis was conducted for each attribute in the database to identify the ranges for each variable to define the archetype structures. One limitation of the database is that it does not differentiate the masonry brick material. However, CM houses with clay units were considered for the proposed archetype houses, as clay units are the most common masonry units in the country, according to data from Portilla et al. (2025). Regarding the roof and slab type, archetype houses were categorized as having rigid diaphragms, flexible diaphragms, or no diaphragms (lightweight roofs). In typical

Table 1. Quality levels represented by f'_m of CM archetypes

Number of stories	Low level (MPa)	Intermediate level (MPa)	High level (MPa)
1	2.0	3.5	5.0
2	3.5	5.0	6.5
3 and 4	4.5	6.0	7.5

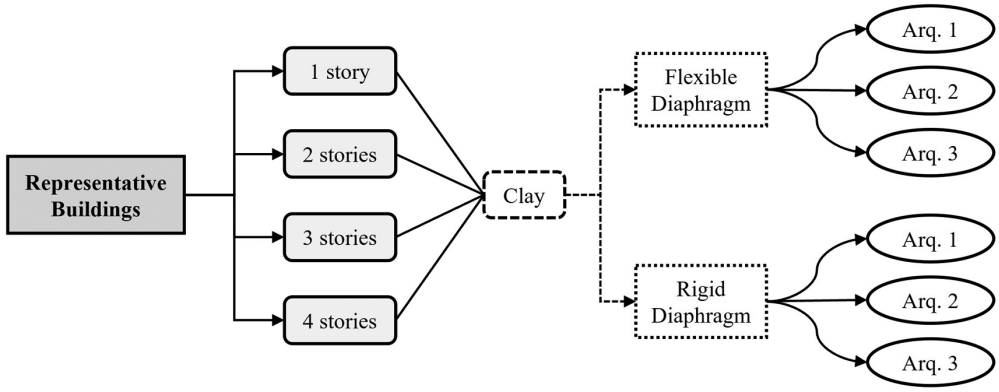

Figure 2. Definition of the archetype houses scheme.

CM houses, diaphragms can vary depending on construction materials. Floor and roof slabs built with RC are typically considered rigid diaphragms, due to their high in-plane stiffness. In contrast, lightweight roofs constructed with timber, or light-gauge steel elements are classified as flexible diaphragms, given their lower in-plane stiffness. The quality and strength of masonry units were accounted for by varying the compressive strength of the masonry, f'_m, defining three different quality levels for houses with one, two, three, and four stories, as shown in Table 1. The dimensions and detailing of the confining elements in the CM walls were designed following the latest Colombian building code requirements for earthquake-resistant construction NSR-10 (AIS, 2010).

Figure 2 presents all possible combinations resulting from the attributes considered for one- to four-story houses. The compressive strength of the masonry was also varied according to the proposed performance levels for each architectural configuration. In total, 72 archetype houses were obtained by summing all possible combinations.

Despite the limited size of the database, the archetype buildings were chosen from different regions of the country. Data obtained from literature review (Acevedo et al., 2020; Maldonado Rondón and Chio-Cho, 2008; Yamín and García, 1992) provided information about the range of floors and wall distribution for CM buildings across various regions in Colombia. The selected geometric properties for the archetypes were constrained to fall within the interquartile range (i.e. between quartiles one and three) of the box and whisker plots presented in Figure 3. Wall densities (W.D.) were considered in both the transverse (width) and longitudinal (length) directions of each archetype. Figure 3 shows that CM dwellings typically have floor areas of less than 100 m^2 and inter-story heights between 2.3 and 2.6 m. To facilitate identification, archetype houses were labeled using the following system: ARQ#_H#_fm#_D$, where ARQ is the architecture plan number which is

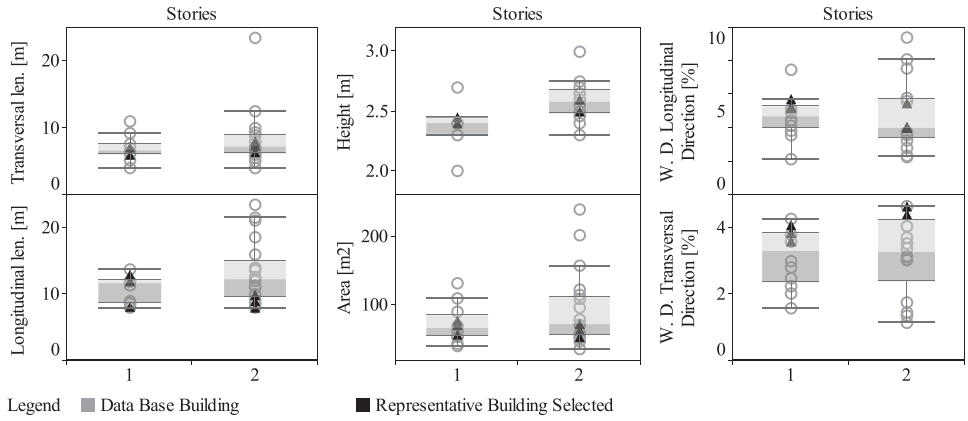

Figure 3. Archetype houses variability in terms of database houses.

associated with predefined wall densities in X and Y direction, and is specified in the database of the archetypes, H is the number of stories, fm is the masonry compressive strength (f'_m), and D$ denotes either DF (flexible diaphragm) or DR (rigid diaphragm). A set of schematic representations of all archetype buildings, including 3D views, floor plans, elevations, and key structural and material properties, is included in the Supplementary Material of this article.

Ground motion selection

The present study uses a ground motion selection methodology called the Conditional Scenario Spectra (CSS), first proposed by Abrahamson and Al Atik (2010). The CSS methodology allows the selection of ground motions in a hazard-consistent approach. Moreover, the CSS are a set of realistic ground-motion spectra with assigned rates of occurrence that reproduce the hazard at a site of interest over a range of hazard levels (return periods) and a range of structural periods (Arteta and Abrahamson, 2019).

The CSS procedure follows the methodology described by Arteta and Abrahamson (2019), in which Uniform Hazard Spectra (UHS) are first calculated for a range of return periods. Conditional Mean Spectra (CMS) are then computed following (Baker, 2011), and used to guide the selection of ground motions whose spectral shapes are consistent with both the CMS and its variability (Jayaram et al., 2011). The CMS is conditioned on a target spectral acceleration value at the period of interest, commonly referred to as the conditioning period (T*) (Baker, 2011). Ground motions are then scaled and assigned occurrence rates to match the hazard across all periods and levels.

A set of ground motions was selected to be consistent with the seismic hazard in several principal cities of Colombia. In this study, the ground motions selected for the cities of Barranquilla, Bogota, and Cali were used, representing cities in low, intermediate, and high seismicity zones, respectively. Finally, the hazard calculation was carried out for eight return periods and nine conditional structural periods (T*), as shown in Table 2. Figure 4 presents the UHS of the three cities and some of the response spectra of the ground motions selected using the CSS.

Table 2. Discretization of the hazard performed for the selection of accelerograms

Parameter	Description
Return period, TR [Years]	[75, 150, 225, 475, 975, 2475, 4975, 9975]
Soil types	[Rock, Soil] = $\left[Vs_{30} \geqslant 760\frac{m}{s}, 360\frac{m}{s} \geqslant Vs_{30} \geqslant 180\frac{m}{s}\right]$
Conditional periods T* [s]	[0.01, 0.1, 0.3, 0.6, 0.7, 1.0, 1.5, 2.0, 3.0]

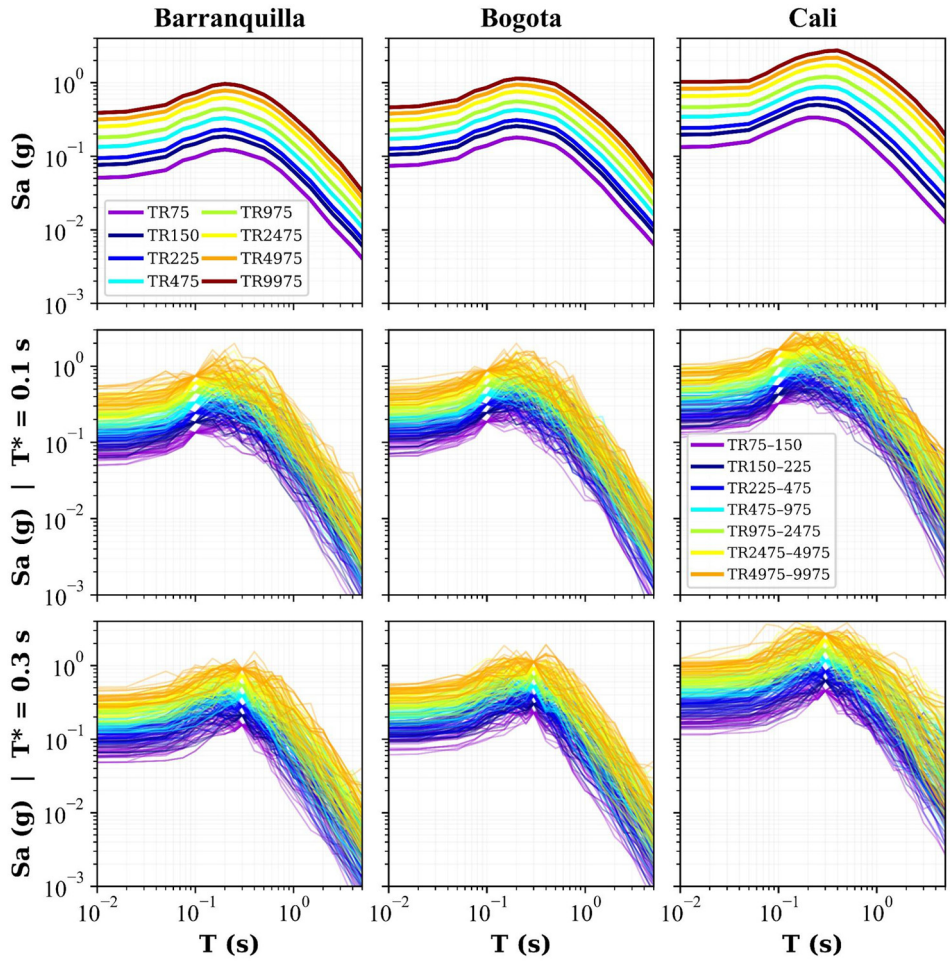

Figure 4. UHS and corresponding response spectra for ground motions with different hazard levels in three cities: Barranquilla, Bogotá, and Cali.

The intensity measure (IM) used to estimate the fragility of CM is the pseudo-spectral acceleration at the fundamental period ($Sa[T_1]$). Given that this research aims to develop fragility function for houses of different number of stories, the choice of the conditioning period of the CSS will be the closest to the fundamental period of these houses. Thus, for one- and two-story houses $Sa(T = 0.1\,s)$ is used, and for three- and four-story houses $Sa(T = 0.3\,s)$ is used.

In the end, for each city, the ground motion set includes approximately 3000 to 3500 signals in total, which corresponds to an average of 425 to 500 horizontal ground motion records per hazard level and conditioning period (Arroyo et al., 2025). These records were selected in pairs to form two-component time histories, with each pair consisting of two orthogonal horizontal components from the same event. The vertical component of ground motion was not considered in this study.

Nonlinear numerical models

Masonry is an anisotropic and highly nonlinear material. Its behavior is highly affected by attributes such as the mortar used and the type of masonry unit. However, micro-models that detail each of these attributes result in high computational costs and demand numerous input parameters, which are not always straightforward to define or estimate.

As an alternative to micro-models, macro-models can effectively represent the seismic behavior of structures, particularly for understanding the global response of the structure. The novel V-D strut model proposed by Borah et al. (2021) was used to model the archetype houses. This methodology incorporates lateral load resistance with a diagonal strut, as other authors have implemented (Raka et al., 2015; Rankawat et al., 2021; Torrisi et al., 2012). In addition, it explicitly models a more realistic axial force distribution among the masonry wall and the tie columns with the presence of a vertical strut. Given that the archetypes will be subjected to lateral loads in both directions during the seismic analysis, a modification to the original model of Borah et al. (2021) was proposed in this study. The modification involves an additional diagonal strut to account for the reversed cyclic loading, as shown in Figure 5.

Inelastic models

The proposed Modified V-D Strut Model was implemented in OpenSees (McKenna et al., 2010). These numerical models were then calibrated with 14 experimental tests on single CM walls performed by different authors (Arias Acosta, 2005; Borah et al., 2021; Cruz Sagastume, 2013; San Bartolomé et al., 2013; Singhal and Rai, 2018). Furthermore, 3D models were calibrated using the experimental results reported by Arias Acosta (2005).

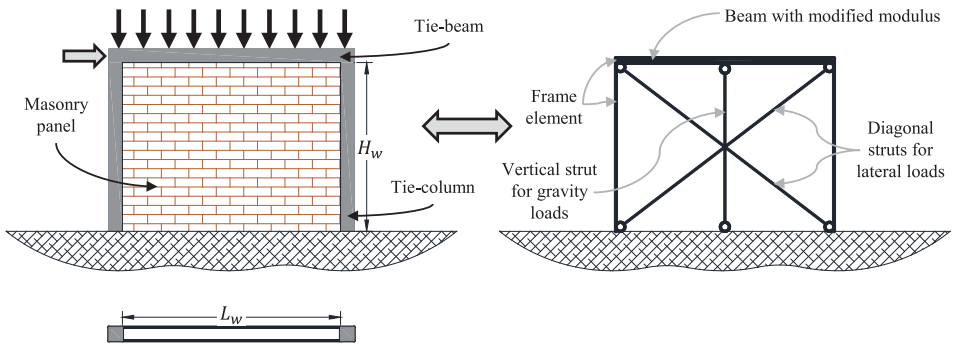

Figure 5. Modified V-D strut model proposed.
Adapted from Borah et al. (2021).

Table 3. Material properties used in the inelastic models

Material	Value adopted	References
Concrete	$f'_c = 21\ MPa$, $\varepsilon_{c_0} = 0.0020$ $G_{fc} = 25N/m$, $E_c = 4400\sqrt{f'_c}$ $f_{t_c} = 0.10f'_c$, $E_{ts} = 0.10\left(\frac{2f'_c}{\varepsilon_{c0}}\right)$ $G_c = 0.4E_c$	Guerrero et al. (2022) Pugh et al. (2015)
Steel	f_y= 442 MPa, ε_y = 0.0029 $f_{s_{ut}} = 636\ MPa$, $\varepsilon_{s_{ut}} = 0.07$ $f_{suc} = 487\ MPa$, $\varepsilon_{s_{uc}} = 0.02$ $\varepsilon_{s_{maxt}} = 0.1$, $\varepsilon_{s_{maxc}} = 0.1$	Carrillo et al. (2021) Carrillo et al. (2023)
Masonry	$f'_m = 2.0 - 7.5\ MPa$, $\varepsilon_{m_0} = 0.003$ $E_m = 622f'_m$ for horizontal perforation units $E_m = 775f'_m$ for vertical perforation and solid units $f_{t_m} = 0.08\,f'_m$ $f_{m_u} = 0.60f'_m$, $\varepsilon_{m_u} = 0.006$	Kaushik et al. (2007) Guerrero et al. (2022) Borah et al. (2021)

Table 3 summarizes the main material properties and modeling parameters used in this study. Additional details and assumptions are described below.

Each CM panel is modeled with three frame elements (two tie columns and one tie beam) and three struts (two diagonal and one vertical strut), as shown in Figure 5. Tie columns were modeled using standard nonlinear elements (forceBeamColumn) with distributed plasticity and fiber sections at the integration points (Spacone et al., 1996). Second-order P-Δ effects were considered in these tie columns using the Corotational formulation (see Section 6.3.1 of Filippou and Fenves [2004]). Concrete was modeled as unconfined, because tie elements do not have confinement zones in the transversal reinforcing detailing, using the uniaxial material Concrete02IS available in OpenSees. The linear softening post-peak branch of the concrete model was regularized according to Coleman and Spacone (2001) to enforce objectivity in the local and global post-peak response. The fracture energy of concrete (G_{fc}) in compression (Jansen and Shah, 1997) was taken as 25 N/mm for unconfined concrete, as suggested by Pugh et al. (2015). This fracture energy is defined here from the peak stress until the end of the f'_c softening branch in the stress-strain curve multiplied by the length of the integration point L_{IP}. The strain corresponding to the compressive strength f'_c was taken as $\varepsilon_{c_0} = 0.0020$ and the elastic modulus E_c was estimated as $E_c = 4400\sqrt{f'_c}$ according to Guerrero et al. (2022). The tensile strength of the concrete, f_{t_c}, was assumed as $0.10f'_c$, and the tension softening stiffness, E_{ts}, was estimated as $E_{ts} = 0.10\left(\frac{2f'_c}{\varepsilon_{c0}}\right)$. The concrete strength used for CM tie columns was 21 MPa according to the information collected in the database. In addition, the uncracked shear modulus of concrete was taken as $G_c = 0.4E_c$.

The stress-strain behavior of the reinforcing steel was modeled using the uniaxial *Hysteretic* material implemented in OpenSees. This formulation requires the maximum strength, initial stiffness, ultimate strain, yielding, softening, and hardening of the steel as input parameters. For the monotonic yield capacity of the reinforcement bars commercialized in Colombia, the values reported by Carrillo et al. (2021) and Carrillo et al. (2023) were used; the yield stress of the steel and the yield strain were taken as f_y = 442 MPa and ε_y = 0.0029, respectively. Also, the maximum tensile capacity was defined as

$f_{s_{ut}} = 636\,MPa$, and the associated strain for this was set at $\varepsilon_{s_{ut}} = 0.07$ to account for the failure by rupture of the steel bar. Conversely, the maximum compressive capacity was set as $f_{suc} = 487\,MPa$, and was defined with an associated strain of $\varepsilon_{s_{uc}} = 0.02$ to consider the potential failure by buckling of the longitudinal bars, as stated by Carrillo et al. (2023). A failure strain was defined as 0.1 for the reinforcement steel according to Carrillo et al. (2021). The remaining parameters to model the hysteretic response of the material were set following the guidelines of Mazzoni et al. (2007), and the failure was modeled using the *MinMax* wrapper.

Due to the high stiffness of the tie beam resulting from the presence of the masonry wall that restricts its vertical displacement (Borah, 2021) and considering that the slab can be used as a horizontal confinement element, this element was modeled as an elastic element using the command *ElasticBeamColumn*. Borah (2021) conducted a parametric analysis using finite element models to determine the effective width of the vertical strut and a modification factor for the modulus of elasticity that would result in deflection values for the confinement beam consistent with experimental results. As a result, these authors found that the tie beam would have a modified modulus of elasticity equivalent to 20 times its actual modulus of elasticity, that is, $20E_b$, and the vertical strut would have an equivalent width of $0.75L_w$, where L_w is the length of the CM wall excluding the tie-columns. The thickness of the vertical strut corresponds to the thickness of the wall. The area of the strut is estimated as the width times the thickness of the vertical strut. The vertical strut was modeled as a truss element. For masonry, the uniaxial material *Concrete02IS* proposed by Kent and Park (1971) and modified by Scott et al. (1982) was used. In the case of the vertical strut, the associated compressive strength was that of masonry, denoted as f'_m, and the associated strain at this strength was $\varepsilon_{m_0} = 0.003$ according to Kaushik et al. (2007). Similarly, the modulus of elasticity proposed by Guerrero et al. (2022) was used, where $E_m = 622f'_m$ for masonry with horizontal perforation units; and $E_m = 775f'_m$ for units with vertical perforation and solid units. Finally, the tensile strength of masonry was chosen as $f_{t_m} = 0.08f'_m$ based on the suggestion of Borah et al. (2021). The ultimate compressive strain of masonry was set to $\varepsilon_{m_u} = 0.006$ and the corresponding stress is $0.20f'_m$ (Kaushik et al., 2007).

The diagonal struts provide the lateral resistance of the CM wall. The lateral strength of this diagonal strut is not the same as the compressive strength of the masonry because of the different possible failure modes. Borah et al. (2021) argued that a brittle shear failure at the brick-mortar interface in the form of bed joint sliding or stepped cracks or a combination are the predominant failure modes under lateral loads usually observed in CM houses. Therefore, the diagonal strut strength corresponds to the weakest possible failure mode; in this study, this parameter is called the effective shear strength of masonry, f_{ss} and it is estimated with Equation **1** or **2** depending in the aspect ratio (AR) (Borah, 2021). The thickness of the diagonal strut is equal to the nominal thickness of the masonry units, while the width is equal to $1/3\,L_d$, where L_d is the length of the diagonal strut according to the analysis performed by Borah et al. (2021). The area of the strut is estimated as the width times the thickness of the diagonal strut. The loads applied to each CM node were obtained from the ETABS model, CSI (2015) and then exported to OpenSees. The structural response of the CM walls is influenced by the axial load since the f_{ss} is proportional to the vertical stress in the wall (σ), as well as other variables as the thickness of the wall (t), the longitudinal reinforcement ratio in tie-columns (ρ_l), the f'_m and f'_c of the tie elements. The influence of axial load on lateral behavior has been noted in the literature; for instance, Tarque et al. (2022) reported that while axial load increases lateral strength, it also reduces displacement

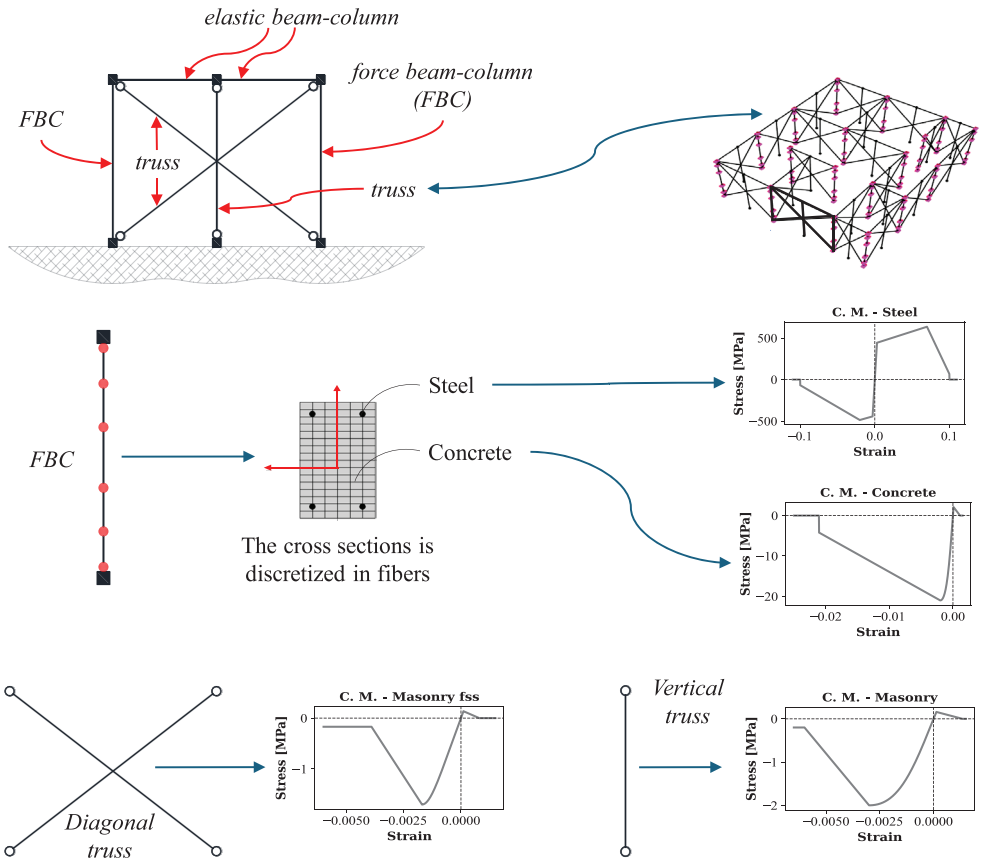

Figure 6. Modified equivalent V-D strut model for CM houses.

capacity, making CM walls more brittle. For each one of the walls the level of axial load was estimated using ETABS and with this data the calculation of the f_{ss} was done. This ensures that the mechanical properties of each wall in the numerical model—at all story levels—are updated in terms of the corresponding axial load. For the archetypes in this study, the vertical stress in the walls ranged between 0 MPa (no axial load) to 0.586 MPa. The mass used for the dynamic analysis corresponds to the dead load and 25% of the live load. A summary of the configuration of the model that represents a single CM wall is presented in Figure 6. To consider openings due to doors or windows, a reduced factor (FR) of the effective shear strength was estimated using Equation 3:

$$f_{ss} = 0.096t^{0.217} f'^{0.827}_{m} f'^{0.081}_{c} \rho_l^{0.018} (1+\sigma)^{0.235} AR^{0.101} \quad if\ AR \leqslant 1 \tag{1}$$

$$f_{ss} = \frac{0.134t^{0.133} f'^{0.886}_{m} f'^{0.107}_{c} \rho_l^{0.002} (1+\sigma)^{0.004}}{AR^{0.248}} \quad if\ AR > 1 \tag{2}$$

$$FR = 0.6A_r^2 - 1.6A_r + 1 \tag{3}$$

where A_r is the ratio between the opening area and the wall area (Singhal and Rai, 2018). The walls should not have significant openings to ensure satisfactory earthquake performance. It is important to note that AIS (2010) limits the openings in CM walls to 30% of the wall area.

Due to its complexity and the high computation cost, soil-structure interaction was not considered in this study. Furthermore, nodes at ground level were modeled as fixed. As previously mentioned, the archetype houses floor systems were modeled under two conditions: as rigid diaphragm and as flexible diaphragm. For the rigid diaphragm models, in-plane displacements of all nodes at each floor level were constrained to move together in OpenSees by applying multi-point constraints (RigidDiaphragm command) among all nodes at each diaphragm level. For the models with a flexible diaphragm, the diaphragm was modeled as a shell element (*ShellMITC4* in OpenSees) with mechanical properties $E_c = 20{,}000$ MPa using $4400\sqrt{f'_c}$, a Poisson coefficient of 0.20 and thickness of the slab of 0.10 m. Considering post-earthquake surveys and past experimental studies, Kollerathu and Menon (2017) stated that flexible diaphragms significantly alter the seismic behavior of masonry structures. The roof of the archetypes with flexible diaphragm is modeled without constraints, which means that the displacement of each node is independent of the others.

Calibration and validation of inelastic models

The validation of the models was performed for different types of masonry units (hollow, tubular, or solid) and were done at two levels: at the element level (for a single CM walls), and at the structure level (for scaled CM houses). In these calibrations, adjustment factors for the properties of the constitutive curve of the effective shear resistance were estimated. An effective area factor (FA_{ss}) was estimated for hollow and tubular masonry units to account for the reduced area that transfers the loads, due to the holes in the bricks. This effective area factor was applied to the transversal area of the strut. The adjustment and effective area factors are shown in Table 4.

The first set of single CM wall specimens to be calibrated were those with hollow masonry bricks reported by Cruz Sagastume (2013). The experimental program included seven wall specimens; however, only five single CM wall panels (ME1, ME2, ME3, ME4, and ME5) were chosen in this study. The aspect ratios of the five full-scale CM walls ranged between 0.6 and 2.2, and all were constructed with a height of 2.5 m, including the slab. In addition, the thickness used for the masonry and the columns was 0.12 m, and the width of the columns was 0.15 m. The walls were subjected to cyclic loads applied in a pseudo-static manner. Figure 7 shows that the analytical model (orange curve) fits well with the experimental model (black curve).

Table 4. Masonry adjustment factors for the diagonal strut constitutive model

Unit type	$F\varepsilon_{c_{0ss}}$	$F\varepsilon_{c_{u\,ss}}$	$FE_{m\,ss}$	FA_{ss}
Solid	$0.89 - 0.15AR$	1.00	0.50 *if* $AR \leq 1.5$ 0.90 *if* $AR > 1.5$	1.00
Hollow	$0.94 - 0.12AR$	0.80	0.50	$0.90 - 0.15AR$
Tubular	$0.86 - 0.18AR$	0.65	1.00	$0.88 - 0.18AR$

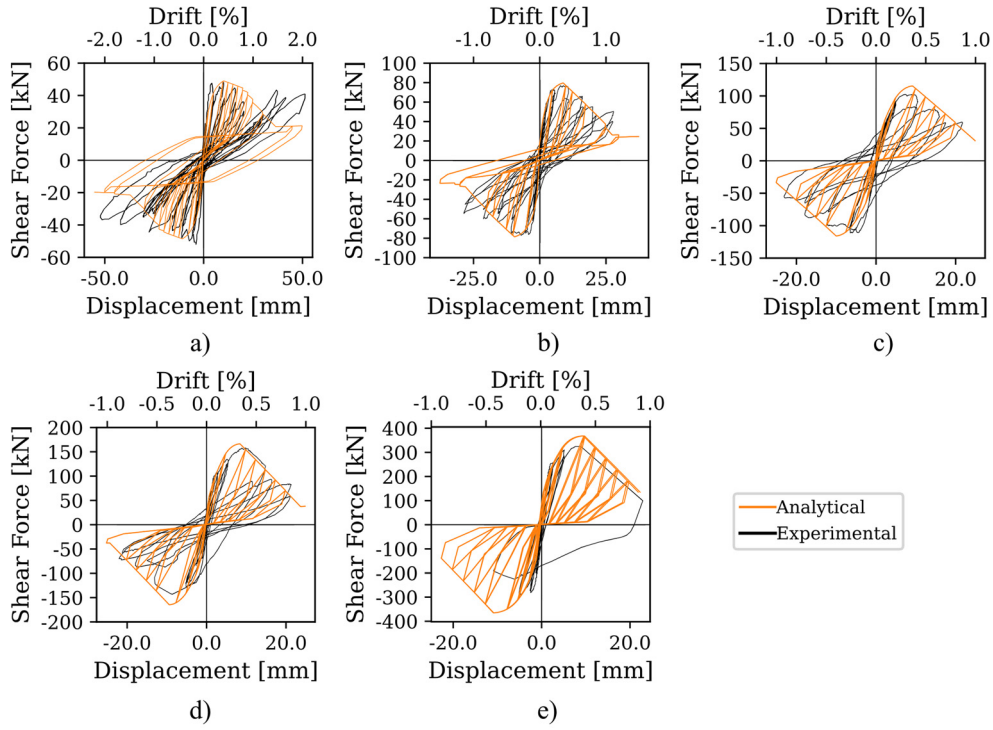

Figure 7. Comparison between measured and predicted response of CM walls with hollow bricks: (a) ME1, (b) ME2, (c) ME3, (d) ME4, and (e) ME5.

The calibration of the solid masonry wall bricks was carried out using the specimens reported by Borah et al. (2021). A group of four specimens (ME1, ME2, ME3, and ME4) with aspect ratios ranging from 1.04 to 2.75 were chosen from their experimental campaign. All of them were constructed with a height of 2.34 m, including the slab. In addition, the thickness used for both the masonry and the columns was 0.12 m, and the width of the column was 0.15 m. The walls were subjected to pseudo-static cyclic loads. The envelope of the cyclic response was recovered and compared with the response obtained from the pushover analysis obtained from the nonlinear analytical model, as observed in Figure 8. This figure shows that the analytical model (orange curve) fits well with the initial stiffness of the elastic part of the experimental model (black curve).

Finally, a set of calibrations of CM walls with tubular bricks were conducted. This masonry unit type is frequently used in Colombia and thus, it was used to model most of the archetypes of one and two stories considering that tubular units are only permitted for these number of floors. On the other hand, hollow and solid bricks were used in three and four-story houses. Two specimens were chosen independently: W1 (San Bartolomé et al., 2013) and MTUB (Diaz et al., 2017). In both cases, the tie-columns included transverse reinforcement through stirrups: Bartolomé et al. used #2 stirrups and Díaz et al. used #1 stirrups, spaced at 10 cm near the joints and at 25 cm in the remaining length of the columns. The response of specimen W1 is shown in Figure 9a. The analytical model (orange curve) generally fits the elastic and plastic parts well and correctly predicts peak deformation and shear base values as well as the corresponding deformation. The response of

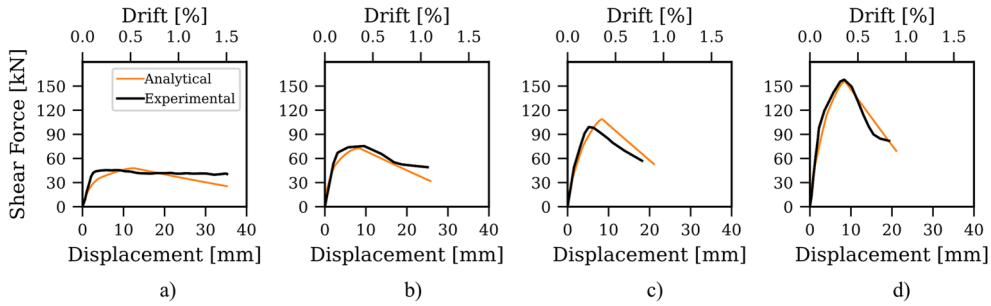

Figure 8. Comparison between the envelope of the experimental cyclic response and the pushover curves from the nonlinear analytical models for CM walls with solid bricks: (a) ME1, (b) ME2, (c) ME3, and (d) ME4.

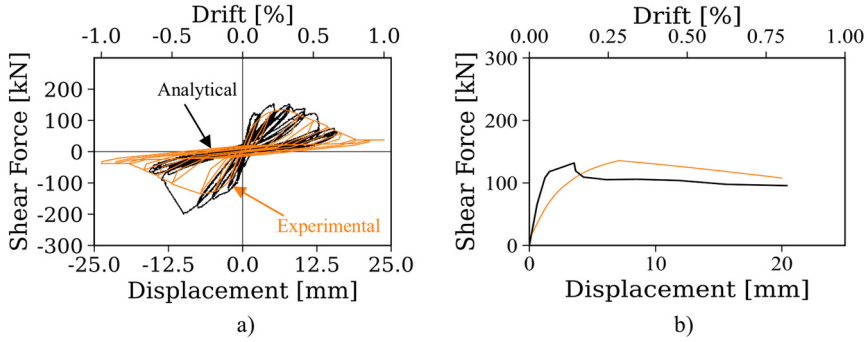

Figure 9. Calibration for CM walls with tubular bricks: (a) W1 (San Bartolomé et al., 2013) and (b) MTUB (Diaz et al., 2017).

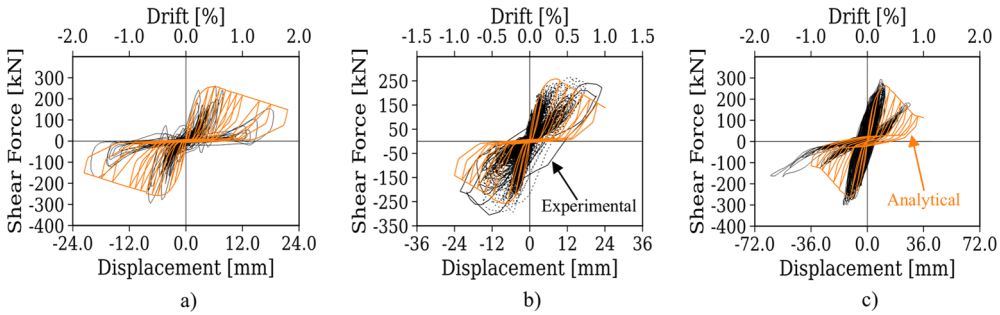

Figure 10. Lateral load-displacement relationship of CM houses: (a) one-story, (b) two-story, and (c) three-story.

specimen MTUB is presented in Figure 9b. In this case, the analytical model (orange curve) acceptably fits and accurately predicts peak shear force, and the load-displacement envelope approximates the experimental one (black curve).

In the final step in the calibration process, three CM buildings of one, two, and three stories tested by Arias Acosta (2005) were used to validate the proposed nonlinear model for these 3D specimens. As shown in Figure 10, the hysteretic response from the numerical

models and the target experimental curves yields good agreement both in the plastic branch of the curve and in the stiffness degradation branch. The constitutive variables besides f_{ss} used to define the constitutive relationship of the diagonal struts are obtained multiplying the masonry constitutive variables by its adjustment factors obtained from the calibrations and that were previously shown in Table 4.

Fragility analysis

A fragility function shows the probability of exceeding a damage state (DS) given an *IM* value. A fragility analysis is performed in this section to link a given ground motion intensity to the probability of a given CM house reaching or exceeding a specific DS. This analysis requires the definition of an engineering demand parameter (*EDP*) highly correlated with the damage to the CM house under analysis. In this study, the peak inter-story drift ratio (*IDR*), defined as the maximum IDR across all stories in the building, was selected as the EDP to estimate fragility due to its strong correlation with structural damage in confined masonry buildings, as noted by Ruiz-García and Negrete (2009). Using data from experimental tests, these authors established the relationship between wall capacity and stiffness loss at different inter-story drift values. They also demonstrated how factors like axial compressive stress, wall height-to-length ratios, and reinforcement configurations influence structural response.

To assess the fragility of each archetype, the PEER-PBEE methodology was implemented. The PEER-PBEE methodology allows assessing a structure's expected performance in terms of decision variables that are of direct interest to the different stakeholders (Deierlein and Moehle, 2004; Günay and Mosalam, 2013). This can be done using the total probability theorem according to Equation 4. Fragility functions are derived from the convolution of structural response and the variability of the definition of the DSs. This is expressed as follows in Equation 5 and can be expressed in a discrete way using Equation 6; where $P(DS>ds|EDP=edp)$ represents the probability of exceeding a DS given that an *edp* value was reached. Furthermore, $p(EDP|IM)$ is the probability of occurrence of an EDP level given that an IM level has occurred:

$$(DV) = \iiint G\langle DV|DM\rangle dG\langle DM|EDP\rangle dG\langle EDP|IM\rangle d\lambda(IM) \tag{4}$$

$$P(DS>ds|IM) = \int P(DS>ds|EDP)p(EDP=edp|IM) \tag{5}$$

$$P(DS>ds|im_i) = \sum_{j=1}^{m}\left[P\left(DS>ds|edp_j\right)p\left(edp_j|im_i\right)\right] \tag{6}$$

Carrillo and Rincon (2023) compiled DS definitions for CM walls from various studies (Astroza and Schmidt, 2004; Ruiz-García and Negrete, 2009; Tarque et al., 2022). Their review informed the adoption of four DSs for this study, ranging from DS1 (onset of diagonal cracking) to DS4 (collapse). Table 5 summarizes these DS definitions alongside the median IDR values and dispersion parameters (β). In this study, lognormal is the distribution of choice to fit the damage data. This decision is based on its simplicity, the fact that it's been used for decades in the industry to fit fragility data, and more importantly, it seems to fit engineering data relatively well (Porter, 2021). The median values for DS1 and DS2 were adopted from Ruiz-García and Negrete (2009), whose damage state definitions

Table 5. Description of the damage states selected $P[DS \geqslant ds_i|IDR]$.

DS	Description	θ [IDR %]	β
DS1	Onset of diagonal cracking mechanism	0.16	0.40
DS2	Diagonal cracks can be observed. The wall is reparable and minimal damage is observed.	0.27	0.40
DS3	Maximum shear strength is reached. Extensive damage is observed.	0.49	0.40
DS4	Collapse of the wall	0.73	0.40

Adapted from Ruiz-García and Negrete (2009), Tarque et al. (2022), and Astroza and Schmidt (2004).

align with those used in this study. Their experimental data reflect conditions that match the CM walls in the selected archetypes, specifically the presence of axial load and the absence of horizontal reinforcement. The DS3 median value was taken from Tarque et al. (2022), whose DS2 definition corresponds to extensive damage and the attainment of shear capacity, which closely matches our DS3 criteria. Since Astroza and Schmidt (2004) were the only authors to report a median value for the near-collapse limit state, the median proposed in their study was adopted in this work for DS4. All three references used CM wall specimens with axial load levels consistent with those considered in this study ($\sigma_v = 0 - 0.586\,MPa$). A constant dispersion (β) of 0.40 was adopted for all damage states due to the lack of specific dispersion values reported in the literature. This value of 0.40 is within the range of values found in the literature (Ruiz-García and Negrete, 2009; Tarque et al., 2022).

To perform the fragility analysis of the archetypes, first, the structural response of each archetype had to be studied. Each archetype was assigned to one of three representative cities (Barranquilla, Bogotá, and Cali) to reflect low, intermediate, and high seismicity zones. NLTH analyses were performed to obtain EDP vs IM data. Each run used the 3D OpenSees model subjected to bi-directional loading, with a pair of horizontal ground motion components applied simultaneously along the longitudinal and transverse directions of the structure, without enforcing any specific orientation strategy. The vertical component of ground motion was not considered. As previously mentioned, the IM used for one- and two-story houses was $Sa(T = 0.1\,s)$, while for three- and four-story houses, it was $Sa(T = 0.3\,s)$.

From these NLTH runs, sets of EDPs and their corresponding IM are obtained, as shown in the scatter plot of Figure 11a. In this case, as previously discussed, the IM of choice was $S_a(T_1)$; from these scatter plots it can be noted that increasing values of the IM yield increasing EDP levels, as anticipated. However, it is also possible to see in the figure that the dispersion in EDP values grows with larger $S_a(T_1)$, suggesting that this IM might not be an efficient choice to predict the seismic behavior of these type of structures. The efficiency of an IM refers to its ability to minimize the variability of an EDP when subjected to ground motions with the same intensity (Dávalos and Miranda, 2019). Several authors have proposed alternative IMs that could improve efficiency (Baker and Allin Cornell, 2005; Dávalos and Miranda, 2019; Eads et al., 2015; Raghunandan and Liel, 2013). Despite its limitations, $S_a(T_1)$ was selected as the IM based on project-wide decisions made for the National Seismic Risk Model of Colombia. Given the model's nationwide scope, a standardized set of structural periods of interest (0.1 s, 0.3 s, 0.6 s, 1.5 s, and 2.0 s) was established through an analysis of the Global Earthquake Model (GEM) database. These pairs of EDPs vs IM are then binned by intensity level, as shown in Figure 11b.

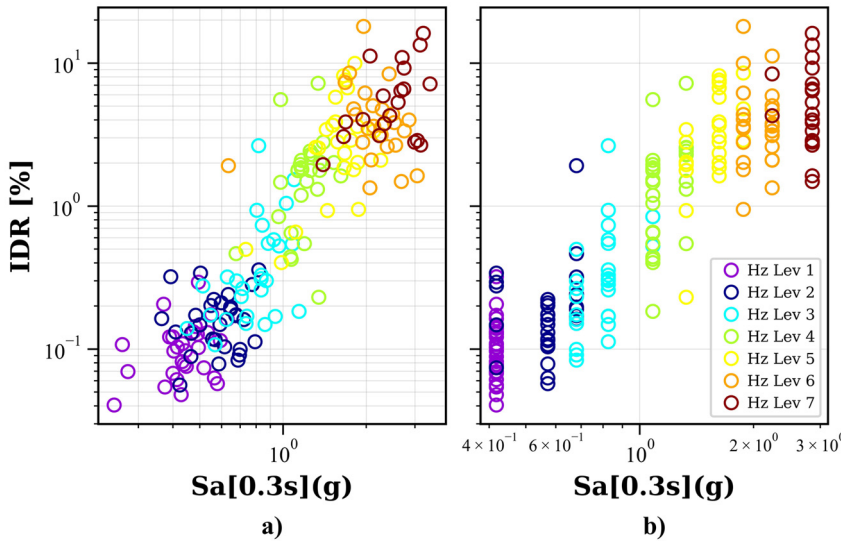

Figure 11. Scatterplot results for model ARQ1_H3_fm7.5_DR for: (a) EDP versus IM and (b) bin data process.

From there, the estimation of fragility functions is straight forward and can be obtained following the methodology presented by Baker (2015) by fitting lognormal distributions to the sorted and binned data. In this figure, "Hz Lev X" refers to the hazard level associated with return period, previously explained in the Ground Motion Selection section of this study, where X ranges from 1 to 7, representing increasing $Sa(T_1)$ levels.

A lognormal distribution of EDP given the value of IM, $p(edp_j|im_i)$ in Equation 5, was estimated for each of the bins. To prevent unrealistic structural responses from biasing the fragility estimation, a data censoring threshold was applied. As Martins and Silva (2021) noted, numerical models can converge at deformation levels that represent complete structural failure but result from model limitations rather than realistic behavior. Following the approach proposed by (Martins and Silva, 2021), who established a threshold at 1.5 times the EDP corresponding to complete damage, a censoring threshold at twice the median IDR for DS4 was defined, which indicates the onset of global collapse. This approach ensures that unrealistically high responses are excluded from the statistical estimation of fragility functions. Then, the results of the convolution of Equation **6** for each DS were adjusted to a cumulative lognormal distribution. Finally, this process is repeated for each archetype. Figure 12 shows fragility curves for archetypes of one story with rigid diaphragm and Figure 13 for flexible diaphragm. It is possible to see that archetypes with flexible diaphragms have lower values of theta, which suggests that these archetypes are more vulnerable to seismic demands.

Finally, fragility curves for the structural typologies were generated. The typologies were named, using a modified version of the GEM taxonomy (Brzev et al., 2013), MA/MC/DMO/H:X, where MA corresponds to masonry, MC to confined masonry, H: X represents the number of stories, and DMO indicates moderate energy dissipation. For

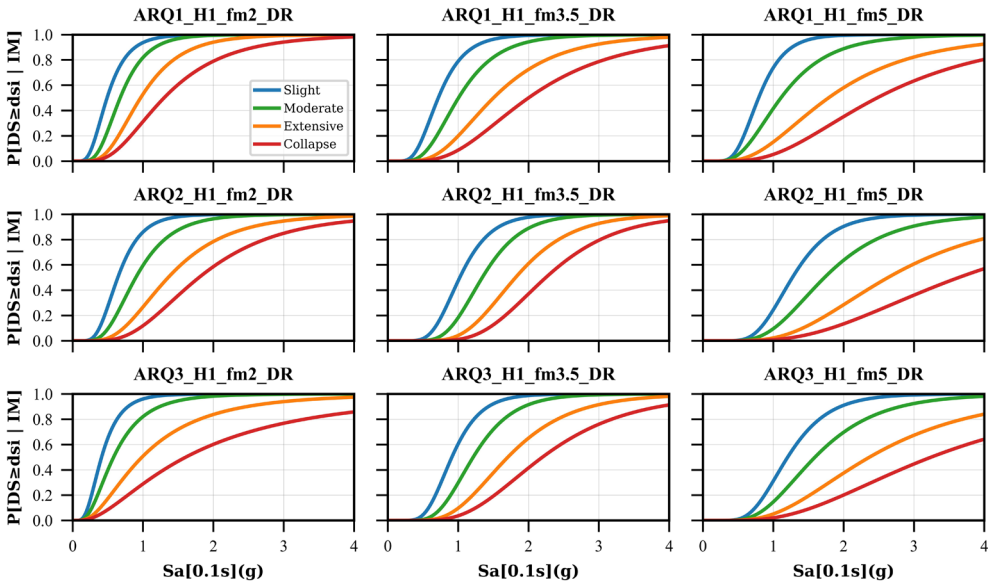

Figure 12. Fragility curves of archetypes of one story with rigid diaphragm.

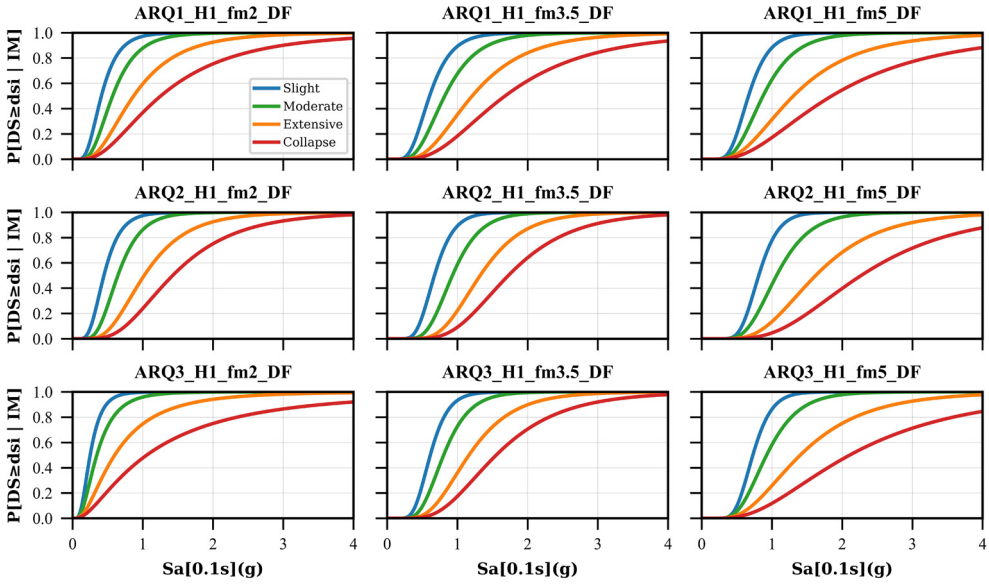

Figure 13. Fragility curves of archetypes of one story with flexible diaphragm.

instance, MA/MC/H:1/DMO represents a one-story CM house with moderate dissipation capacity. The houses' typology fragility curves were estimated by combining the time history analysis data of all the archetype houses that represent the typology. Then, the

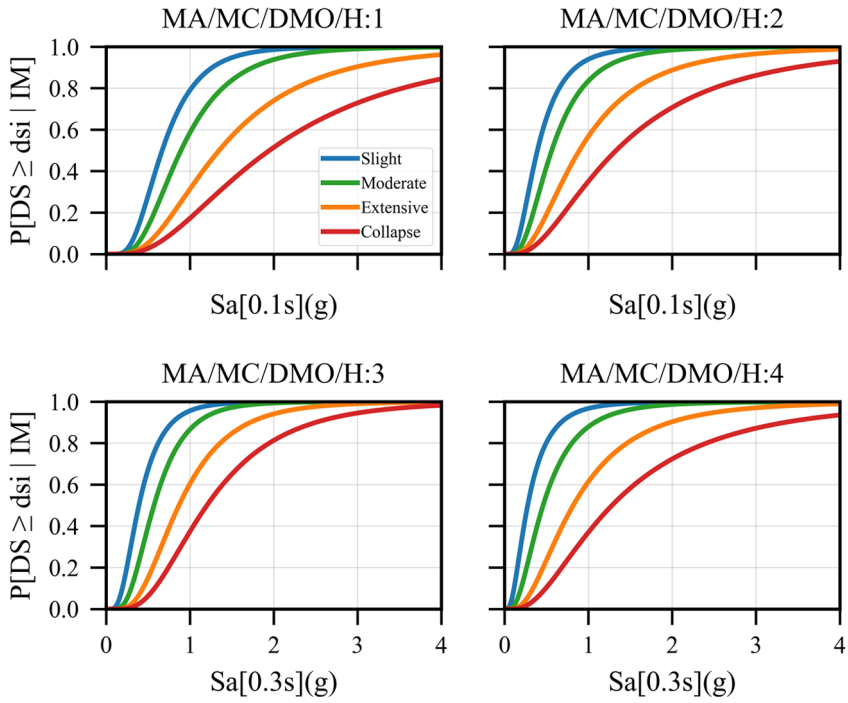

Figure 14. Fragility curves obtained for the CM typologies.

Table 6. Fragility curves of confined masonry houses

Typology	IM (*g*)	Parameter	DS1	DS2	DS3	DS4
MA/MC/DMO/H:1	Sa(T = 0.1 s)	θ [*g*]	0.67	0.89	1.35	1.95
		β	0.50	0.52	0.61	0.71
MA/MC/DMO/H:2	Sa(T = 0.1 s)	θ [*g*]	0.42	0.59	0.93	1.38
		β	0.58	0.58	0.65	0.75
MA/MC/DMO/H:3	Sa(T = 0.3 s)	θ [*g*]	0.39	0.57	0.87	1.20
		β	0.55	0.51	0.53	0.57
MA/MC/DMO/H:4	Sa(T = 0.3 s)	θ [*g*]	0.28	0.46	0.82	1.28
		β	0.70	0.66	0.69	0.75

application of the methodology previously explained in this section, namely, using Equation 6 for the combined data were performed, obtaining the typology fragility curves as shown in Figure 14. The median and standard deviation defining the fragility functions for each of the typologies were obtained and are presented in Table 6, and in Figure 14.

Results in Figure 14 allow to compare the fragility curves with the same IM, for example, MA/MC/DMO/H:1 with MA/MC/DMO/H:2 or MA/MC/DMO/H:3 with MA/MC/DMO/H:4. CM houses of one story have a lower probability of exceeding a DS when compared to CM houses of two stories. Similarly, MA/MC/DMO/H:3 performs seismically better than MA/MC/DMO/H:4, as indicated by their higher median Sa(T) values across

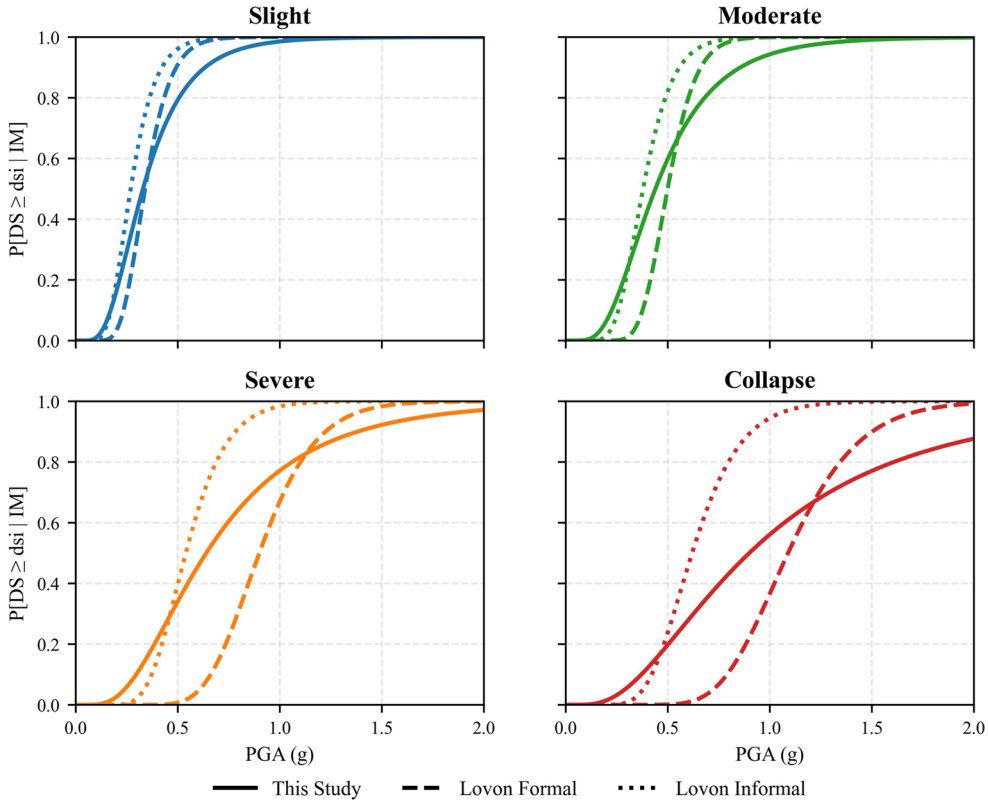

Figure 15. Comparison of fragility functions for one-story CM houses with curves developed by Lovon et al. (2018).

all DSs. This suggests that three-story houses require stronger ground shaking to reach the same level of damage, including collapse. The standard deviation of all the collapse fragility curves estimated is higher than that of the other DS. One explanation associated with increasing dispersion is the lack of collapse data for high *IM* values. The uncertainty in the building response near the collapse could also impact the dispersion of the data.

The fragility curves of CM houses were compared with the fragility curves of other typologies of the MNRS. Furthermore, a comparison with the results of other authors who developed fragility curves of CM walls was also performed. Figures 15 and 16 compares CM fragility curves with the ones estimated by Lovon et al. (2018). In the study by Lovon et al., both formal and informal CM dwellings were studied. Due to differences in the IM used between this study and Lovon et al. (2018), the fragility curves may vary. Thus, the fragility curves of the current study were recalculated with PGA and Sa [0.2 s], which was the IM used by Lovon et al. for one-story and two-story CM houses respectively. The results indicate that CM buildings in Colombia lie between the formal and informal fragility curves reported by Lovon et al. This could be attributed to the widespread use of tubular clay bricks in Colombia, which often exhibit low compressive strength.

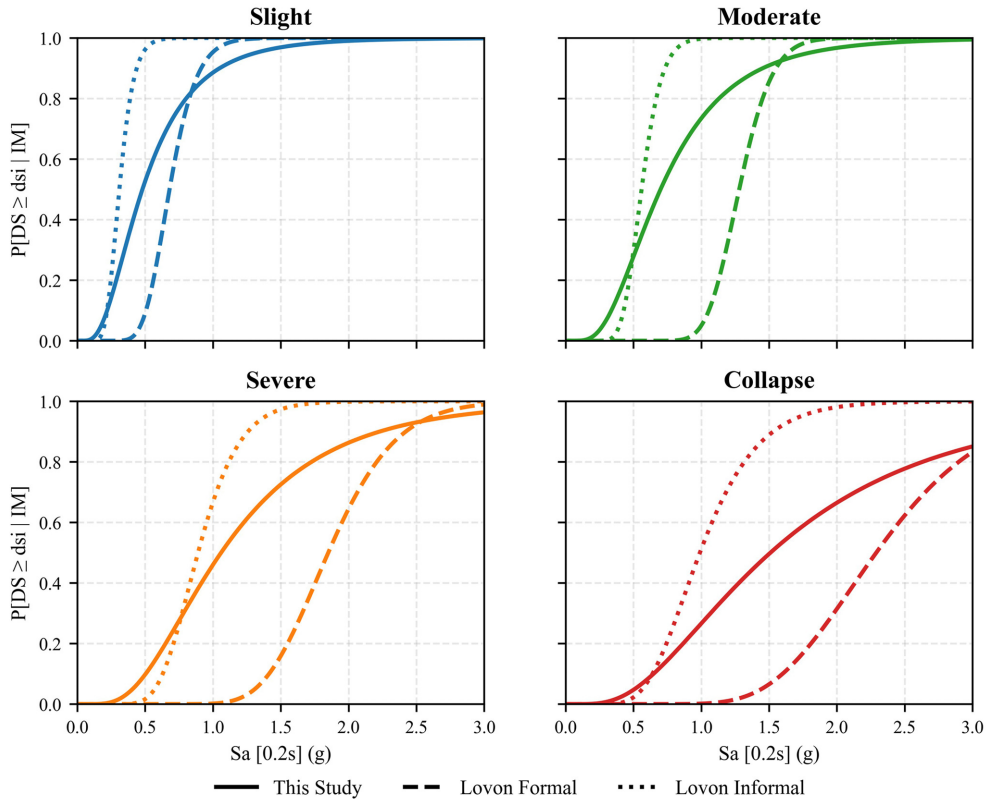

Figure 16. Comparison of fragility functions for two-story CM houses with curves developed by Lovon et al. (2018).

Concluding remarks

CM buildings are widely used in Latin America and other emerging countries. The extensive use of CM houses underscores the importance of understanding their seismic behavior to anticipate potential structural and societal consequences. In this study, seismic fragility curves were developed to assess the fragility of CM buildings in Colombia. A country-specific database of CM buildings was compiled, and 72 archetypes representing common CM construction practices were proposed and analyzed to ensure the robustness of the fragility assessment.

The archetypes were modeled using a modified version of the "Equivalent V-D Strut Model," proposed by Borah et al. (2021). This study modified the macro-model to incorporate 3D structural models, considering alterations in strength due to wall openings. It accounts for the gravitational effects of permanent loads and seismic forces derived from selected accelerograms. These archetypes were evaluated through nonlinear time history analyses using approximately 370 ground motion records consistent with the seismicity of three main cities: Barranquilla, Bogota, and Cali. Furthermore, the models were validated against experimental data, including quasi-static cyclic tests and scaled shaking table tests, ensuring consistency with observed structural behaviors.

The fragility analysis revealed several important trends. As expected, shorter CM buildings, particularly one- and two-story houses, demonstrated lower probabilities of severe DSs, such as extensive damage or collapse. This improved seismic performance was attributed to their reduced seismic demands and better force distribution. In contrast, taller structures, including three- and four-story houses, exhibited higher fragility due to increased mass and reduced wall density, which amplified seismic effects. Material properties, such as masonry compressive strength, were found to play a critical role in seismic performance; houses constructed with stronger masonry units showed significantly lower probabilities of collapse compared to those with weaker materials. In addition, diaphragm rigidity had a marked impact on fragility, with rigid diaphragms offering better seismic performance than flexible ones across all damage states.

The study underscores the importance of refining the Colombian seismic code (NSR-10) to address the specific vulnerabilities of CM buildings. Current code provisions should be revisited to include minimum requirements for tie column dimensions, masonry material quality, and wall opening allowances, which could significantly reduce fragility and enhance seismic performance.

While the fragility curves developed in this study are specific to Colombia, they hold broader relevance for other Latin American countries with similar construction practices and seismic conditions. By leveraging these findings, future studies can expand the understanding of CM fragility and its implications for seismic risk across the region.

This research also highlights opportunities for further advancements. Expanding the regional database to include more diverse archetypes could capture additional variations in construction practices across Colombia. Conducting experimental tests on CM walls built with local materials would provide critical data to refine damage state definitions and improve fragility assessments. Incorporating spatial arrangements of archetypes in future simulations would better represent collective seismic behaviors in urban environments.

The fragility curves developed in this study represent a critical input for Colombia's National Seismic Risk Model, supporting efforts to improve seismic safety and reduce vulnerabilities associated with future earthquakes. By addressing region-specific fragility and advancing the understanding of CM seismic performance, this study contributes to broader disaster resilience initiatives in Colombia and beyond.

Acknowledgments

The work presented in this paper has been developed within the framework of the Special Cooperation Agreement No. 018 of 2021 between the Colombian Geological Survey and the Colombian Association of Engineering Faculties (ACOFI), with financial resources from the National General Budget and the General System of Royalties, and in-kind contributions from ACOFI and the participating universities. Authors also acknowledge to Universidad de Norte (Barranquilla, Colombia) and Universidad Militar Nueva Granada (Bogotá, Colombia) for facilitating or financing research activities.

Declaration of conflicting interests

The authors declared no potential conflicts of interest with respect to the research, authorship, and/or publication of this article.

Funding

The authors received no financial support for the research, authorship, and/or publication of this article.

ORCID iDs

Jorge Archbold https://orcid.org/0000-0001-5461-9181
Julian Carrillo https://orcid.org/0000-0002-8274-5414
Johnatan Orjuela Mejia https://orcid.org/0009-0005-6857-1621

Data availability statement

All supporting data are provided as Supplementary Material. Supplemental Appendix A presents the database compiled to characterize the confined masonry typology, including building attributes such as number of stories, dimensions, wall areas, material properties, and construction details. Supplemental Appendix B includes schematic representations of all archetype buildings, featuring 3D views, floor plans, elevations, and key structural and material properties. Supplemental Appendix C provides the variables and attribute values used in the definition of each archetype.

Supplemental material

Supplemental material for this article is available online.

References

Abrahamson NA and Al Atik L (2010) Scenario spectra for design ground motions and risk calculation. In: *Proceedings of the 9th U.S. national and 10th Canadian conference on earthquake engineering*, 25 July. Available at: https://www.caee.ca/10CCEEpdf/2010EQConf-001896.pdf

Acevedo AB, Yepes-Estrada C, González D, Silva V, Mora M, Arcila M and Posada G (2020) Seismic risk assessment for the residential buildings of the major three cities in Colombia: Bogotá, Medellín, and Cali. *Earthquake Spectra* 36(Suppl. 1): 298–320.

AIS (2010) *Colombian Seismic Design Code: NSR-10*. Bogotá: AIS—Asociación Colombiana de Ingeniería Sísmica.

Arias Acosta JG (2005) *Ensayos en mesa vibradora de un modelo a escala 1:2 de edificio de mampostería confinada de tres niveles* [Master's thesis]. Mexico: Universidad Nacional Autónoma de MéxiCo.

Arroyo O, Bonett R, Vidales F, Ocampo JJ, Feliciano D, Carrillo J and Novoa D (2025) Seismic fragility assessment of reinforced concrete wall buildings in Colombia: Insights and implications for earthquake-resistant design. *Earthquake Spectra* 41(1): 354–380.

Arteta CA and Abrahamson NA (2019) Conditional Scenario Spectra (CSS) for hazard-consistent analysis of engineering systems. *Earthquake Spectra* 35(2): 737–757.

Asfura AP and Flores PJ (1999) *Quindío, Colombia Earthquake of January 25, 1999: Reconnaissance Report (MCEER-99-0017): Multidisciplinary Center for Earthquake Engineering Research (MCEER)*. Available at: https://www.eng.buffalo.edu/mceer-reports/99/99-0017.pdf

Astroza IM and Schmidt AA (2004) Capacidad de deformación de muros de albañilería confinada para distintos niveles de desempeño. *Revista de Ingeniería Sísmica* 70: 59.

Baker JW (2011) Conditional mean spectrum: Tool for ground-motion selection. *Journal of Structural Engineering* 137(3): 322–331.

Baker JW (2015) Efficient analytical fragility function fitting using dynamic structural analysis. *Earthquake Spectra* 31(1): 579–599.

Baker JW and Allin Cornell C (2005) A vector-valued ground motion intensity measure consisting of spectral acceleration and epsilon. *Earthquake Engineering & Structural Dynamics* 34(10): 1193–1217.

Borah B (2021) Seismic analysis and design of confined masonry buildings [Ph.D. thesis, Indian Institute of Technology Guwahati]. Available at: https://repository.iitg.ac.in/handle/123456789/1966

Borah B, Kaushik HB and Singhal V (2021) Development of a novel V-D strut model for seismic analysis of confined masonry buildings. *Journal of Structural Engineering* 147(1): 04021001.

Brzev S, Scawthorn C, Charleson AW, Allen L, Greene M, Jaiswal K and Silva V (2013) *GEM Building Taxonomy Version 2.0 [Pdf]*. GEM Technical Report 2013-02, 188 pages.

Carrillo J, and Rincón R (2023) Modelo de estados límite para componentes estructurales: Reporte MNRS No. 0010-2022. Informe Final [(Servicio Geológico Colombiano (SGC)]. Bogotá: Asociación Colombiana de Facultades de Ingeniería (ACOFI).

Carrillo J, González W and Benjumea J (2023) Cyclic stress–strain behavior of low-diameter reinforcing bars for thin concrete walls. *Bulletin of Earthquake Engineering* 21(12): 5505–5523.

Carrillo J, Lozano H and Arteta C (2021) Mechanical properties of steel reinforcing bars for concrete structures in central Colombia. *Journal of Building Engineering* 33: 101858.

Chung R (1996) *The January 17, 1995 Hyogoken-Nanbu (Kobe) Earthquake* (NIST SP 901; 0 ed., p. NIST SP 901). Gaithersburg, MD: National Institute of Standards and Technology.

Coleman J and Spacone E (2001) Localization issues in force-based frame elements. *Journal of Structural Engineering* 127(11): 1257–1265.

Cruz Sagastume O (2013) *Tests of 7 Full-scale Confined Masonry Walls of Different Lengths with Multi-perforated Clay Units*. Editorial Académica Española. Available at: https://www.amazon.com/dp/3659076279

CSI (2015) *ETABS: Integrated Building Design Software*. Computers and Structures, Inc. Available at: https://www.csiamerica.com/products/etabs

DANE (1999) *Dimensión social y económica de los efectos del terremoto del Eje Cafetero: Diagnóstico para la reconstrucción*. DANE, Bogotá, Colombia.

Dávalos H and Miranda E (2019) Filtered incremental velocity: A novel approach in intensity measures for seismic collapse estimation. *Earthquake Engineering & Structural Dynamics* 48(12): 1384–1405.

Deierlein G and Moehle J (2004) *A Framework Methodology for Performance-based Earthquake Engineering*.

Diaz M, Zavala C, Gallardo J and Lavado L (2017) *Experimental Study of Non-Engineered Confined Masonry Walls Retrofitted With Wire Mesh and Cement-Sand Mortar*.

Dolšek M (2011) Simplified method for seismic risk assessment of buildings with consideration of aleatory and epistemic uncertainty. *Structure and Infrastructure Engineering* 8: 939–953.

Eads L, Miranda E and Lignos DG (2015) Average spectral acceleration as an intensity measure for collapse risk assessment. *Earthquake Engineering & Structural Dynamics* 44(12): 2057–2073.

Eguchi RT, Goltz JD, Taylor CE, Chang SE, Flores PJ, Johnson LA, Seligson HA and Blais NC (1998) Direct economic losses in the Northridge earthquake: A three-year post-event perspective. *Earthquake Spectra* 14(2): 245–264.

Filippou FC and Fenves GL (2004) Methods of analysis for earthquake-resistant structures. In: Bozorgnia Y and Bertero VV (eds) *Earthquake Engineering: From Engineering Seismology to Performance-based Engineering*. Boca Raton, FL: CRC Press, pp. 6–1.

GEM (2022) *OpenQuake Vulnerability and Fragility Documentation*. Available at: https://docs.openquake.org/vulnerability/fragility/index.html

Gonzales GH, Aguilar AG, Huaco G and Garber D (2020) Seismic performance and fragility functions of confined masonry old infrastructure with handmade bricks. *IOP Conference Series: Materials Science and Engineering* 999(1): 012006.

Google LLC (2023) Google street view. Available at: https://www.google.com/maps

Guerrero F, Ortiz AR and Carrillo J (2022) Bayesian uncertainty assessment for modulus of elasticity of concrete and mechanical properties of steel reinforcing bar. In: Noh HY, Whelan M and Harvey PS (eds) *Dynamics of Civil Structures, Volume 2: Proceedings of the 40th IMAC, a conference and exposition on structural dynamics 2022*. Cham: Springer, pp. 101–109.

Günay S and Mosalam KM (2013) PEER performance-based earthquake engineering methodology, revisited. *Journal of Earthquake Engineering* 17(6): 829–858.

Jansen DC and Shah SP (1997) Effect of length on compressive strain softening of concrete. *Journal of Engineering Mechanics* 123(1): 25–35.

Jayaram N, Lin T and Baker JW (2011) A computationally efficient ground-motion selection algorithm for matching a target response spectrum mean and variance. *Earthquake Spectra* 27(3): 797–815.

Kaushik HB, Rai DC and Jain SK (2007) Stress-strain characteristics of clay brick masonry under uniaxial compression. *Journal of Materials in Civil Engineering* 19(9): 728–739.

Kent DC and Park R (1971) Flexural members with confined concrete. *Journal of the Structural Division* 97(3): 1969–1990.

Kollerathu JA and Menon A (2017) Role of diaphragm flexibility modelling in seismic analysis of existing masonry structures. *Structures* 11: 22–39.

Lovon H, Tarque N, Silva V and Yepes-Estrada C (2018) Development of fragility curves for confined masonry buildings in Lima, Peru. *Earthquake Spectra* 34(3): 1339–1361.

McKenna F, Scott MH and Fenves GL (2010) Nonlinear finite-element analysis software architecture using object composition. *Journal of Computing in Civil Engineering* 24(1): 95–107.

Maldonado Rondón E and Chio Cho G (2008) *Vulnerabilidad Sísmica En Centros Urbanos*. Santander: Ediciones Universidad Industrial de Santander.

Marques R, Pereira JM and Lourenço PB (2020) Lateral in-plane seismic response of confined masonry walls: From numerical to backbone models. *Engineering Structures* 221: 111098.

Martins L and Silva V (2021) Development of a fragility and vulnerability model for global seismic risk analyses. *Bulletin of Earthquake Engineering* 19(15): 6719–6745.

Martins L, Silva V, Marques M, Crowley H and Delgado R (2016) Development and assessment of damage-to-loss models for moment-frame reinforced concrete buildings. *Earthquake Engineering & Structural Dynamics* 45(5): 797–817.

Mazzoni S, McKenna F, Scott MH and Fenves GL (2007) *OpenSees Command Language Manual*. Pacific Earthquake Engineering Research Center, University of California, Berkeley, CA. Available at: https://opensees.berkeley.edu/OpenSees/manuals/usermanual/OpenSeesManual.pdf

Meli R, Brzev S, Astroza M, Boen T, Crisafulli F, Dai J, Farsi M, Hart T, Mebarki A, Moghadam AS, Quiun D, Tomazevic M and Yamin L (2011) *Seismic Design Guide for Low-rise Confined Masonry Buildings*. Confined Masonry Network, Earthquake Engineering Research Institute (EERI); International Association for Earthquake Engineering (IAEE). Available at: https://www.world-housing.net/wp-content/uploads/2011/08/ConfinedMasonryDesignGuide82011.pdf

Porter K (2021) A beginner's guide to fragility, vulnerability, and risk. In: Beer M, Kougioumtzoglou IA, Patelli E and Au IS-K (eds) *Encyclopedia of Earthquake Engineering*. Berlin; Heidelberg: Springer, pp. 1–29.

Portilla S, Reyes JC, Carrillo J and Lasso JE (2025) Mechanical properties of masonry using artificial neural networks. *Earthquake Spectra* 41(2): 1536–1564.

Pugh JS, Lowes LN and Lehman DE (2015) Nonlinear line-element modeling of flexural reinforced concrete walls. *Engineering Structures* 104: 174–192.

Raghunandan M and Liel AB (2013) Effect of ground motion duration on earthquake-induced structural collapse. *Structural Safety* 41: 119–133.

Raka E, Spacone E, Sepe V and Camata G (2015) Advanced frame element for seismic analysis of masonry structures: Model formulation and validation. *Earthquake Engineering & Structural Dynamics* 44(14): 2489–2506.

Rankawat N, Brzev S, Jain SK and Pérez Gavilán JJ (2021) Nonlinear seismic evaluation of confined masonry structures using equivalent truss model. *Engineering Structures* 248: 113114.

Restrepo JI and Cowan HA (2000) The "Eje Cafetero" earthquake, Colombia of January 25, 1999. *Bulletin of the New Zealand Society for Earthquake Engineering* 33(1): 1–29.

Rota M, Penna A and Magenes G (2010) A methodology for deriving analytical fragility curves for masonry buildings based on stochastic nonlinear analyses. *Engineering Structures* 32(5): 1312–1323.

Ruiz-García J and Negrete M (2009) Drift-based fragility assessment of confined masonry walls in seismic zones. *Engineering Structures* 31(1): 170–181.

San Bartolomé A, Quiun D, Araoz T and Velezmoro J (2013, June) Seismic reinforcement of existing walls made of horizontally-hollow bricks. In: *Proceedings of the 12Th Canadian Masonry Symposium*. Available at: https://canadamasonrydesigncentre.com/download/12th_symposium/153.pdf

Scott BD, Park R and Priestley MN (1982) Stress-strain behavior of concrete confined by overlapping hoops at low and high strain rates. *Journal Proceedings* 79(1): 13–27.

Silva V, Crowley H, Pinho R and Varum H (2013) Extending displacement-based earthquake loss assessment (DBELA) for the computation of fragility curves. *Engineering Structures* 56: 343–356.

Singhal V and Rai DC (2018) Behavior of confined masonry walls with openings under in-plane and out-of-plane loads. *Earthquake Spectra* 34(2): 817–841.

Spacone E, Filippou FC and Taucer FF (1996) Fibre beam–column model for non-linear analysis of R/C frames: Part I. Formulation. *Earthquake Engineering & Structural Dynamics* 25(7): 711–725.

Tarque N, Manchego A, Lovón H, Blondet M and Varum H (2022) Experimental in-plane behaviour and drift-based fragility assessment of typical Peruvian confined masonry walls. *Construction and Building Materials* 341: 127893.

Torrisi GS, Crisafulli FJ and Pavese A (2012) An innovative model for the in-plane nonlinear analysis of confined masonry and infilled frame structures. In: *Proceedings of the 15th World Conference on Earthquake Engineering* (15WCEE). Available at: https://www.iitk.ac.in/nicee/wcee/article/WCEE2012_0574.pdf

Ulrich T, Negulescu C and Douglas J (2014) Fragility curves for risk-targeted seismic design maps. *Bulletin of Earthquake Engineering* 12(4): 1479–1491.

Vamvatsikos D and Allin Cornell C (2006) Direct estimation of the seismic demand and capacity of oscillators with multi-linear static pushovers through IDA. *Earthquake Engineering & Structural Dynamics* 35(9): 1097–1117.

Villar-Vega M, Silva V, Crowley H, Yepes C, Tarque N, Acevedo AB, Hube MA, Gustavo CD and María HS (2017) Development of a fragility model for the residential building stock in South America. *Earthquake Spectra* 33(2): 581–604.

Yamín L and García L (1992) *Investigaciones Experimentales Relacionadas Con La Vivienda De Bajo Costo En Colombia* (CR3.1).

Yepes-Estrada C, Silva V, Valcárcel J, Acevedo AB, Tarque N, Hube MA, Coronel G and María HS (2017) Modeling the residential building inventory in South America for seismic risk assessment. *Earthquake Spectra* 33(1): 299–322.